ACS NANO
Cite This: ACS Nano 2020, 14, 620–631
www.acsnano.org

ARTICLE

Smart Nanovesicle-Mediated Immunogenic Cell Death through Tumor Microenvironment Modulation for Effective Photodynamic Immunotherapy

Weijing Yang,[†,‡,∥] Fuwu Zhang,[‡,∥] Hongzhang Deng,[‡] Lisen Lin,[‡] Sheng Wang,[‡] Fei Kang,[‡] Guocan Yu,[‡] Joseph Lau,[‡] Rui Tian,[‡] Mingru Zhang,[‡] Zhantong Wang,[‡] Liangcan He,[‡] Ying Ma,[‡] Gang Niu,[‡] Shuo Hu,[*,†] and Xiaoyuan Chen[*,‡]

[†]Department of PET Center, Xiangya Hospital, Central South University, Changsha 410008, China
[‡]Laboratory of Molecular Imaging and Nanomedicine (LOMIN), National Institute of Biomedical Imaging and Bioengineering (NIBIB), National Institutes of Health (NIH), Bethesda, Maryland 20892, United States

Supporting Information

ABSTRACT: **Combination therapy that could better balance immune activation and suppressive signals holds great potential in cancer immunotherapy. Herein, we serendipitously found that the pH-responsive nanovesicles (pRNVs) self-assembled from block copolymer polyethylene glycol-*b*-cationic polypeptide can not only serve as a nanocarrier but also cause immunogenic cell death (ICD) through preapoptotic exposure of calreticulin. After coencapsulation of a photosensitizer, 2-(1-hexyloxyethyl)-2-devinyl pyropheophorbide-a (HPPH) and an indoleamine 2,3-dioxygenase inhibitor, indoximod (IND), pRNVs/HPPH/IND at a single low dose elicited significant antitumor efficacy and abscopal effect following laser irradiation in a B16F10 melanoma tumor model. Treatment efficacy attributes to three key factors: (i) singlet oxygen generation by HPPH-mediated photodynamic therapy (PDT); (ii) increased dendritic cell (DC) recruitment and immune response provocation after ICD induced by pRNVs and PDT; and (iii) tumor microenvironment modulation by IND via enhancing P-S6K phosphorylation for CD8$^+$ T cell development. This study exploited the nanocarrier to induce ICD for the host's immunity activation. The "all-in-one" smart nanovesicles allow the design of multifunctional materials to strengthen cancer immunotherapy efficacy.**

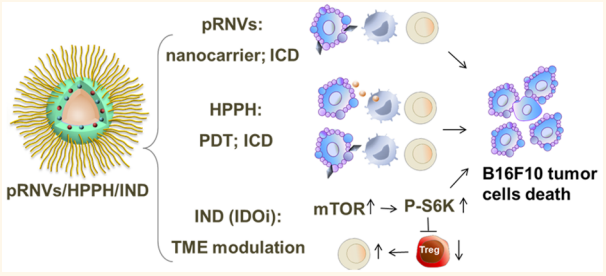

KEYWORDS: *combination therapy, nanovesicle mediated immunogenic cell death, photodynamic therapy, tumor microenvironment modulation, melanoma cancer immunotherapy*

Cancer immunotherapy has been an area of extensive research among the various therapeutic approaches as it can greatly improve clinical outcomes.[1−5] Functional T cells (e.g., CD8$^+$ T cells) are the frontline effectors for inducing tumor cell death. However, their activity is dependent on a myriad of activating and suppressive signals in the tumor microenvironment (TME). Nanotechnology can be used to reliably activate/reinvigorate T cells for combination strategies during cancer immunotherapy.[6−11] Lately, therapeutic approaches, such as immunogenic cell death (ICD), photodynamic therapy (PDT), and inhibition of indoleamine 2, 3-dioxygenase (IDO) activity, have attracted extensive attention in nanotechnology-based cancer immunotherapy.

During the process of ICD, calreticulin (CRT) is translocated to the cell membrane to facilitate dendritic cell (DC) recruitment, recognition, and antigen presentation and strengthen the host's immune response.[12−14] It was reported that certain chemotherapeutic agents (e.g., doxorubicin, oxaliplatin), photodynamic therapy (PDT), photothermal therapy (PTT), and radiotherapy (RT) can induce ICD.[15−20] For example, He *et al.* exploited core−shell nanoparticles to carry oxaliplatin and the photosensitizer pyropheophorbide for cancer immunotherapy.[20] It was observed that reactive oxygen species (ROS) generated by PDT could directly kill tumor cells and that ICD mediated by oxaliplatin and PDT induced CRT exposure and also led to tumor regression.

Received: September 11, 2019
Accepted: December 26, 2019
Published: December 26, 2019

DOI: 10.1021/acsnano.9b07212
ACS Nano 2020, 14, 620−631

Scheme 1. (a) Construction of pH-Responsive Nanovesicles (pRNVs/HPPH/IND) *via* Co-assembly of HPPH, IND, and pH-Responsive Polypeptide.[a] (b) Single Low-Dose *i.v.* Injection of pRNVs/HPPH/IND To Promote Host Immunity and Induce Tumor Cell Death[b]

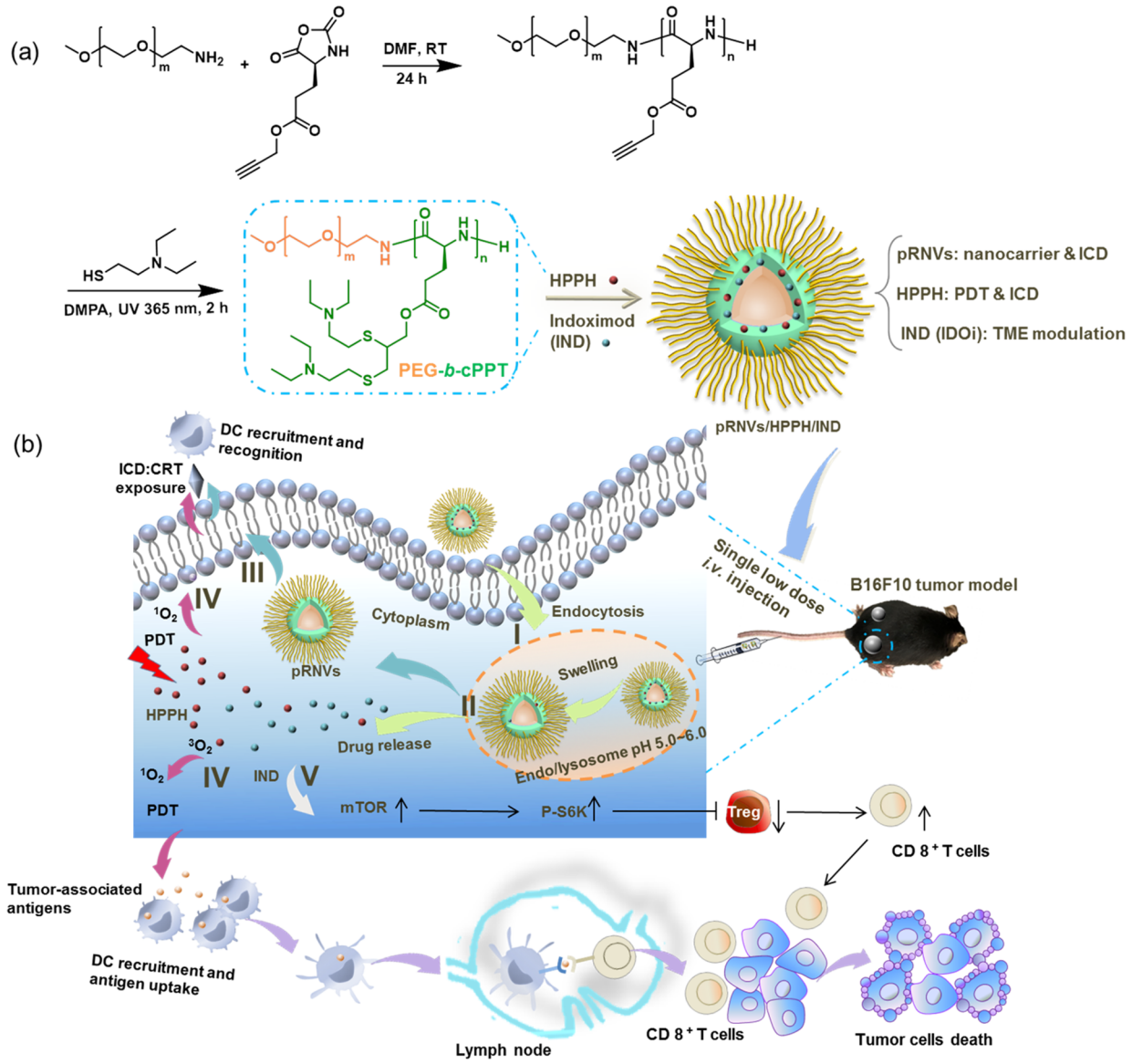

[a]The polypeptide was synthesized by ring-opening polymerization of alkynyl NCA monomer, followed by postpolymerization modification *via* thiol-yne click reaction. [b](I) Internalization of pRNVs/HPPH/IND; (II) swelling and endo/lysosomal escape and of nanovesicles; (III) nanocarrier pRNVs for ICD effect on cancer cell for DC recruitment and recognition; (IV) PDT mediated by HPPH upon laser irradiation, resulting in both ICD effect and directly tumor cells death for TAAs secretion, DC recruitment, maturation, migration, and $CD8^+$ T cell activation; (V) TME modulation by released IND *via* P-S6K1 up-regulation, T_{reg} inhibition, and $CD8^+$ T cell promotion. ICD: immunogenic cell death; PDT: photodynamic therapy; TME: tumor microenvironment.

PDT relies on exogenous light to activate photosensitizer from the ground state to excited state. Energy is transferred to ambient oxygen to produce singlet oxygen ($^1O_2$) or react with substrates accompanied by free radical and radical ion (e.g., $OH^•$, O_2^-) formation, which can cause tumor cell necrosis and apoptosis.[21−24] Given its noninvasiveness and high selectivity, PDT mediated by nanomedicine is an attractive modality for cancer treatment.[25−30] The inflammation response and ICD induced by PDT from ROS-based damage at the endoplasmic reticulum (ER) membrane can recruit dendritic cells (DCs) to tumor tissues and provide additional immune stimuli.[14,22] Recently, extensive work has been reported, where PDT was exploited to enhance cancer immunotherapy.[31−35] For example, Liu *et al.* reported cytomembrane (derived from dendritic cells and cancer cells) coated nanophotosensitizer nanoplatform[36] enabled tumor-specific immunotherapy, with significant abscopal effect, and ICD induced by PDT in the 4T1 breast cancer model.

Immunosuppressive factors present in the TME are considered one of the major obstacles for cancer immunotherapy.[37−41] Recently, IDO inhibitors such as IND and NLG-919 have received extensive attention as immunomodulatory agents.[42−45] The high expression of IDO following interferon γ (IFN-γ) stimulation leads to L-tryptophan overconsumption and kynurenine accumulation in the TME. The depletion of tryptophan can prohibit mTOR pathway interference with P-

DOI: 10.1021/acsnano.9b07212
ACS Nano 2020, 14, 620−631

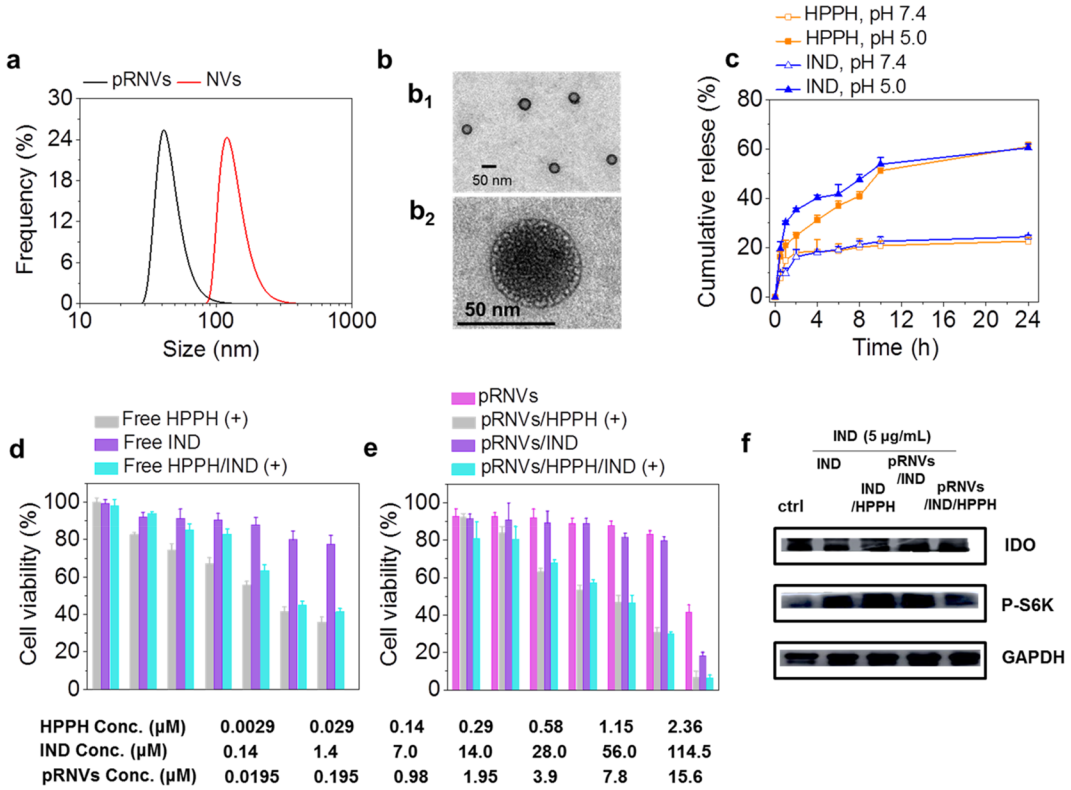

Figure 1. (a) Hydrodynamic size of pRNVs and NVs measured by DLS. (b) TEM (b_1) and cryo-TEM images (b_2) of pRNVs. (c) *In vitro* HPPH and IND release in PBS buffer (pH 7.4) and HAc/NaAc buffer (pH 5.0) over 24 h (n = 3). Cytotoxicity of free drugs (d) and drug nanoformulations (e) against B16F10 cells after 48 h incubation (n = 4). Data are represented as the mean ± SD (f) IDO expression and activation of P-S6K in B16F10 cells after different IND formulation treatment simultaneously with 100 ng/mL IFN-γ stimulation. Control (ctrl) denotes cells just that were only treated with 100 ng/mL IFN-γ. (+) represents that cells were applied with laser irradiation.

S6K phosphorylation, induces regulatory T cells (T_{regs}), and inhibits $CD8^+$ T cell activation.[46−48] IDO has been a popular target to remold the TME and to reinvigorate $CD8^+$ T cells.[42,43,49−51] For example, Lu *et al.* prepared a nanocarrier for the codelivery of oxaliplatin and an IND lipid conjugation to pancreatic ductal adenocarcinoma.[42] IND was able to reverse immune suppression by interfering with IDO pathway and enhance ICD and T lymphocytes infiltration in concert with oxaliplatin.

Herein, we designed a smart nanovesicle self-assembled from pH-responsive block copolymer polyethylene glycol-*b*-cationic polypeptide (PEG-*b*-cPPT). The nanovesicle not only serves as a carrier for therapeutic agents but also intrinsically induces ICD effect to increase immunotherapy efficacy (Scheme 1). Further study indicated that the nanovesicles induced ICD at differential levels across several cancer types. The pH-responsive nanovesicles (pRNVs) were used to encapsulate a photosensitizer (HPPH) and an IDO inhibitor IND via hydrophobic interactions. We hypothesized that the dual-loaded pRNVs (pRNVs/HPPH/IND) would become positively charged in endosomes due to the protonation of tertiary amines in the acidic environment, leading to endosomal escape of pRNV and subsequent release of HPPH and IND in the cytoplasm. After laser irradiation, singlet oxygen mediated by photosensitizer HPPH can directly kill cancer cells by PDT. On the other hand, we anticipated that our smart nanovesicle platform pRNVs/HPPH/IND would also evoke host immunity. The inflammation response mediated by PDT facilitates DC recruitment to tumor sites. The ICD effect induced by both PDT and nanocarrier promotes DC recognition for CRT exposure, followed by DC maturation, migration and antigen presentation to T cells for immune system activation. Moreover, the released IND from pRNVs can restore mTOR pathway with phosphorylation of P-S6K for TME modulation, which eventually stimulates $CD8^+$ T cells (Scheme 1). The multifunctional nanovesicle, which serves as a smart nanocarrier that directly induces ICD effect in combination with PDT and tumor microenvironment modulation, provide the huge potential of nanomaterial design for cancer immunotherapy.

RESULTS AND DISCUSSION

Synthesis of Copolymer, Preparation, and pH Responsibility of pRNVs. The biocompatible polypeptide-based block copolymer was synthesized by ring-opening polymerization of alkynyl *N*-carboxyanhydride (NCA) followed by postpolymerization modification *via* a thiol−yne reaction (Scheme 1a).[52,53] The ^{1}H NMR spectra revealed that the NCA-monomer and polypeptide copolymer were successfully synthesized (Figures S1−S3). According to Figure S3, the molecular weights of the two components in the block copolymer were 5.0 kDa for the hydrophilic PEG and 10.5 kDa for the relatively hydrophobic PPT. The ratio between hydrophilic and hydrophobic segments favors the formation of nanovesicles.[54] As shown in Figure 1a, pRNVs self-assembled into nanovesicles with a hydrodynamic diameter of 55 nm (Table S1) and TEM revealed a hollow structure (Figure 1b). Figure S4 demonstrates that pRNVs undergo swelling and aggregation in acidic aqueous solution, with diameter sizes increasing from 70 to 50, 1500, and 8000 nm in

DOI: 10.1021/acsnano.9b07212
ACS Nano 2020, 14, 620−631

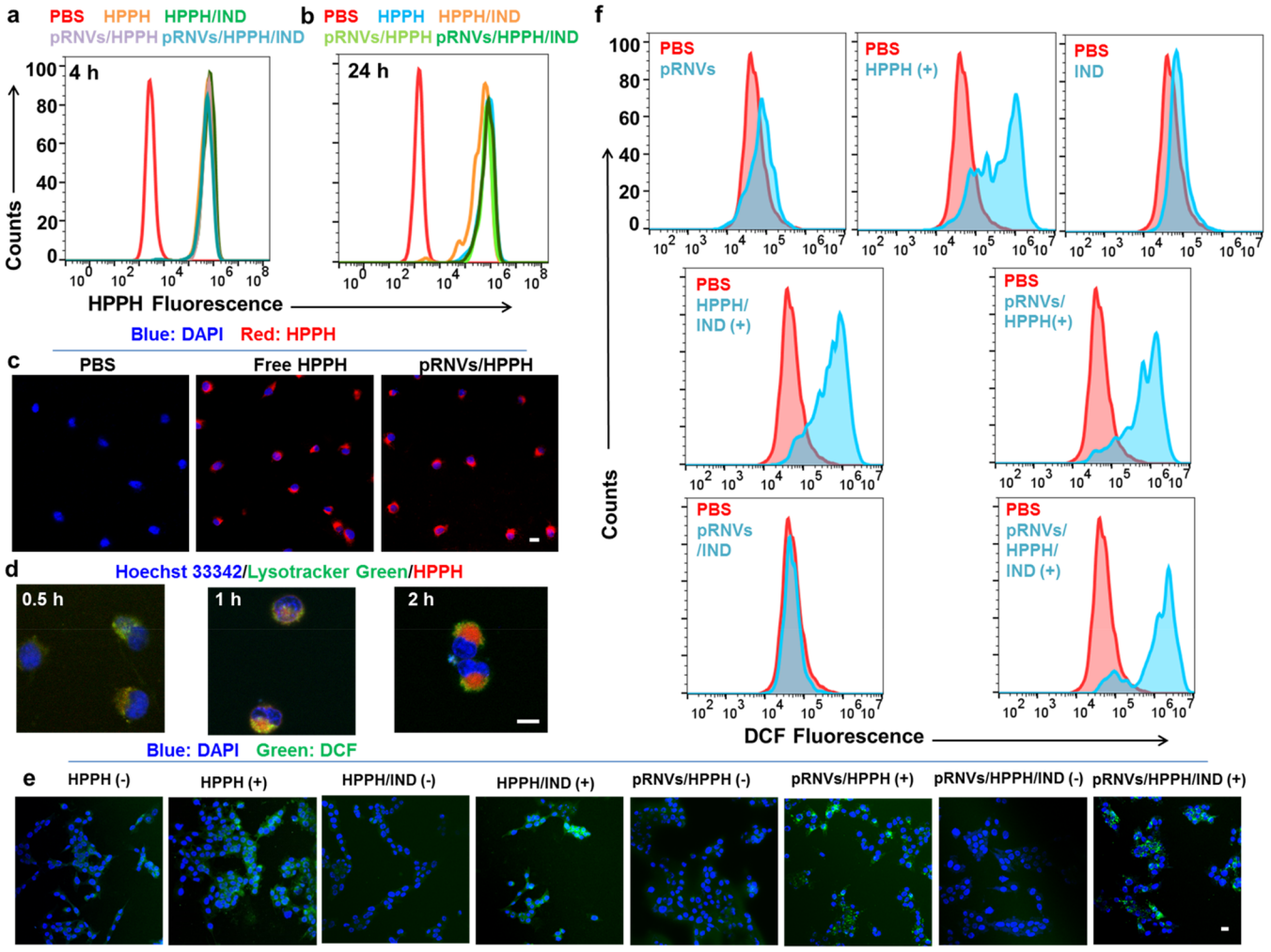

Figure 2. Cellular uptake of different drug formulations in B16F10 cells after 4 h (a) and 24 h (b) incubation measured by flow cytometry. (c) Cellular uptake of free HPPH, and pRNVs/HPPH after 4 h incubation imaged by confocal laser scanning microscope (CLSM). Cell nuclei were stained with DAPI (blue). (d) Endo/lysosomal escape of pRNVs/HPPH at 0.5, 1, and 2 h in B16F10 cells. Cell nuclei were stained with Hoechst (blue); Endosome was stained with Lysotracker Green (green); red fluorescence was from HPPH. (e, f) ROS generation of B16F10 cells after incubation with different treatment formulations by CLSM imaging and flow cytometry. Cell nuclei were stained with DAPI (blue); DCFH-DA was used as a fluorescence probe to detect ROS generation. Scale bars: 20 μm. Symbol (−) and (+) denote without and with laser irradiation at 671 nm (100 mW/cm^2, 1 min).

pH 5.0 after 1, 4, and 12 h incubation. At physiological pH and weak acidic environment, the size change was smaller indicating better stability.

***In Vitro* Drug Release from pRNVs/HPPH/IND, Cytotoxicity, and IDO Activity Test.** As shown in Tables S2 and S3, pRNVs had high drug loading efficiency for both HPPH and IND. We proceeded to investigate drug release at different pH values. It was found that approximately 20% drug released in 24 h in PBS buffer (pH 7.4, 10 mM, 150 mM NaCl), while ~60% drug release was observed in acetate buffer (pH 5.0, 10 mM,150 mM NaCl) (Figure 1c). We determined cell viability for B16F10 cells after 48 h treatment with different formulations by thiazolyl blue tetrazolium bromide (MTT) assays. With laser irradiation, HPPH formulations caused severe cytotoxicities both in B16F10 cells (Figure 1d,e) and 4T1 cells (Figure S8). Notably, HPPH nanoformulations encapsulating both pRNVs/HPPH and pRNVs/HPPH/IND elicited greater B16F10 other than 4T1 cell death compared with free HPPH and HPPH/IND, possibly due to the specific ICD effect of pRNVs in B16F10 cells exacerbating the toxicity. Formulations with only IND were found to have very low potency. Cell viability was less than 40% for empty pRNVs in B16F10 cells and around 65% in 4T1 cells at the highest concentration after 48 h incubation, partially due to cationic charge of the carrier and the ICD effect selectively in B16F10 cells as discussed. Interestingly, pRNVs also have slight adjuvant function, which can promote DC maturation and antigen cross-presentation (Figure S5). Figure S6 showed that more IDO expression was observed with increasing IFN-γ concentrations in B16F10 cells. At the same IFN-γ concentration, addition of IND did not affect IDO expression (Figure 1f and Figure S7). On the other hand, the phosphorylation of S6K was observed in B16F10 and 4T1 cells only after IND treatment. This observation lends support that our strategy can potentially be used to reinvigorate CD8$^+$ T cells (Figure 1f and Figures S7 and S8c).

Cellular Internalization and Endo/Lysosomal Escape of pRNVs/HPPH for B16F10 Cells. Encouraged by the *in vitro* cytotoxicity of pRNVs/HPPH/IND, we further investigated their propensity for internalization and endo/lysosomal

DOI: 10.1021/acsnano.9b07212
ACS Nano 2020, 14, 620−631

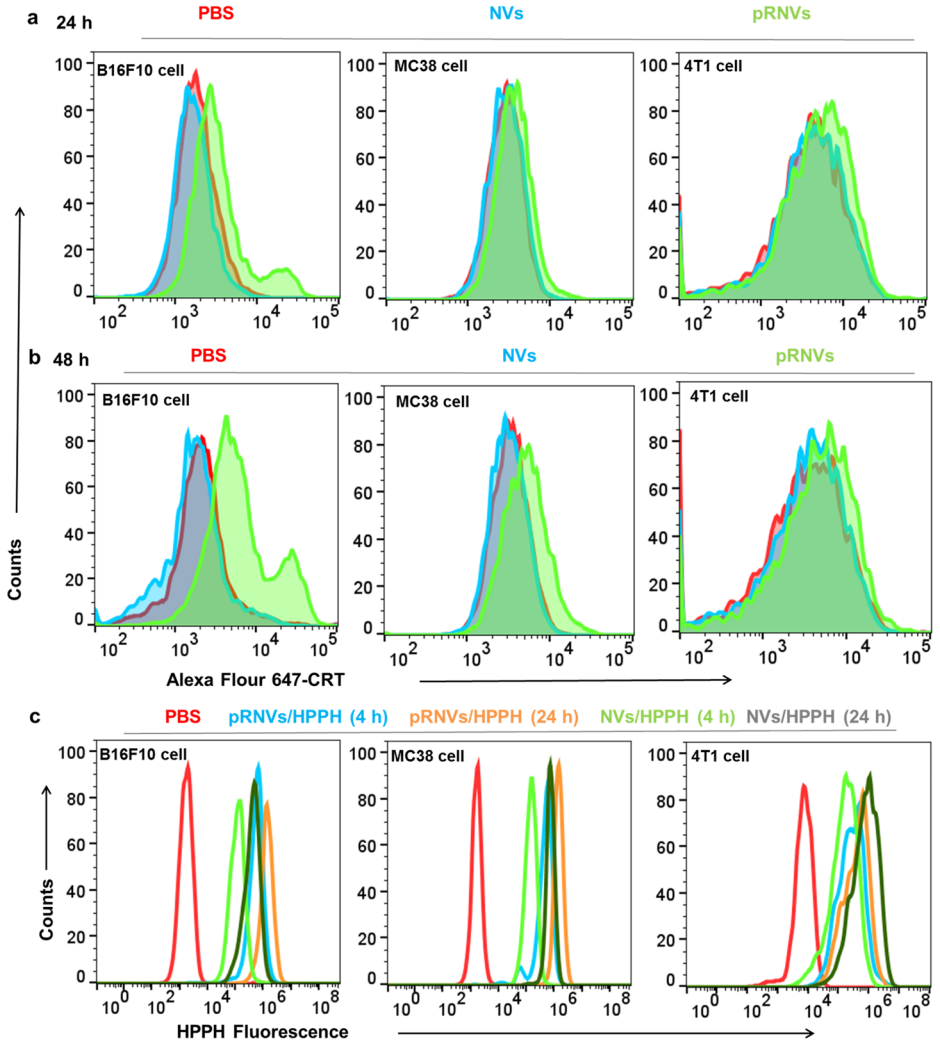

Figure 3. (a, b) ICD effect of NVs and pRNVs on B16F10, MC38, and 4T1 cells after 24 and 48 h incubation, respectively. (c) Cellular uptake of NVs/HPPH and pRNVs/HPPH in B16F10, MC38, and 4T1 cells.

escape. Comparable red fluorescence (HPPH) intensity was observed in B16F10 cells for free HPPH and different HPPH loaded nanoformulations after 4 h treatment (Figure 2a,c and Figure S9), and fluorescent images revealed internalization of the constructs (Figure 2c and Figure S10). When the incubation time was increased to 24 h, intracellular HPPH fluorescence for B16F10 cells was similar to 4 h treatment for all groups, suggesting that the uptake and internalization occurred mainly within the initial 4 h (Figure 2b and Figure S9). Due to the size differences between NVs and pRNVs, we then explored the cellular uptake mechanism of the two nanoparticles. According to Figure S11, cellular internalization of both NVs and pRNVs is energy dependent and is actively endocytosed *via* clathrin- and caveolin-mediated pathways. We then investigated whether pRNVs could effectively escape from endosomes using pRNVs/HPPH as an example. According to Figure 2d and Figure S13, even as early as 0.5 h, pRNVs were partially uptaken by B16F10 cells. Weak red fluorescence (HPPH) was observed with limited colocalization with endo/lysosome. At 1 h, more colocalization (yellow color) appeared, indicating that pRNVs were trapped in the endo/lysosome compartment. Finally, pRNVs escaped from endo/lysosomes with separation and reemergence of the red HPPH and lysotracker green signals at 2 h, suggesting possible drug delivery to cytoplasm. As a matter of fact, Cy5-labeled pRNVs eventually localized in endoplasmic reticulum after fast escape from endo/lysosome (Figure S12).

ROS Generation of HPPH Formulations for PDT in B16F10 Cells. PDT contributes to tumor cell death by generating singlet oxygen for direct tumoricidal effects and by inducing ICD with immune response activation. According to Figure 2e and Figure S14, HPPH formulations generated reactive oxygen species (ROS) in B16F10 cells after laser irradiation (671 nm, 100 mW/cm^2, 1 min), as represented by the strong DCF fluorescence signal. Neither the pRNVs nor IND alone could generate detectable levels of ROS at the same conditions. Without laser irradiation, weak DCF fluorescence was detected for HPPH formulations probably because of dark toxicity (Figure 2e and Figure S14). HPPH-mediated ROS generation was also confirmed by flow cytometry. According to Figure 2f and Figure S15, B16F10 cells treated with HPPH formulations had higher ROS level for strong DCF fluorescence observed after laser irradiation (671 nm, 100 mW/cm^2, 1 min) compared to PBS control

ICD Effect of pRNVs Alone in Different Cells and Possible Mechanism Investigation. ICD plays a pivotal role in killing tumor cells and eliciting the host immune system. In B16F10 cells, we observed CRT expression

DOI: 10.1021/acsnano.9b07212
ACS Nano 2020, 14, 620−631

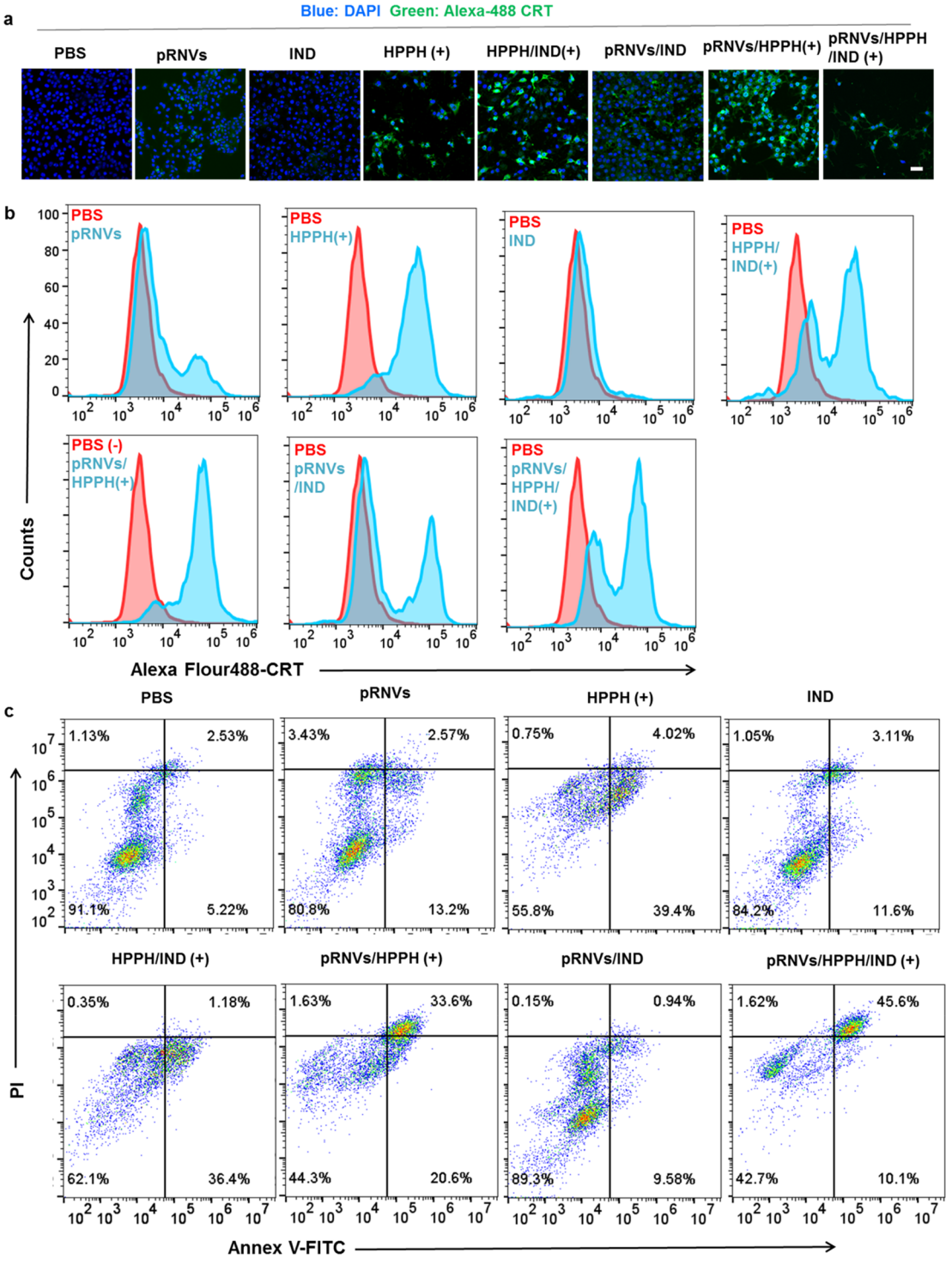

Figure 4. ICD effect of drug loaded nanovesicles on B16F10 cells after 24 h incubation by CLSM (a) and flow cytometry (b) characterization. Cell nuclei were stained with DAPI (blue); CRT was stained with Alexa-488 (green). Scale bar: 40 μm. (c) Apoptosis in B16F10 cells induced by different formulation *via* flow cytometry. Symbol (+) denotes laser irradiation at 671 nm (100 mW/cm^2, 1 min). Annex V-FITC staining was used for early apoptosis and propidium iodine staining for late apoptosis.

following treatment with pRNVs alone that increased at longer incubation time from 1.6- (24 h) to 2.4-fold (48 h), even 15.8-fold increment for partially treated cells at 48 h (Figure 3a,b and Figure S16a,b). However, this effect was cell line dependent, as pRNVs induced minimal (1.5-fold at 48 h) to no expression of CRT in MC38 cells and 4T1 cells (Figure 3a,b and Figure S16a,b). Nanovesicles (NVs) self-assembled from nonresponsive block copolymers PEG-*b*-PPT did not induce ICD in B16F10, MC38, and 4T1 cells. Even though cellular uptake of NVs/HPPH was slightly less than pRNVs/HPPH at 4 h, fluorescence intensity was similar to the latter at 24 h in all three cell lines (Figure 3c and Figure S16c). The data indicated that B16F10 cells may be more sensitive to the pH-responsive tertiary amine or thiol ether groups for ICD by CRT exposure. This is an interesting finding which broadens

DOI: 10.1021/acsnano.9b07212
ACS Nano 2020, 14, 620−631

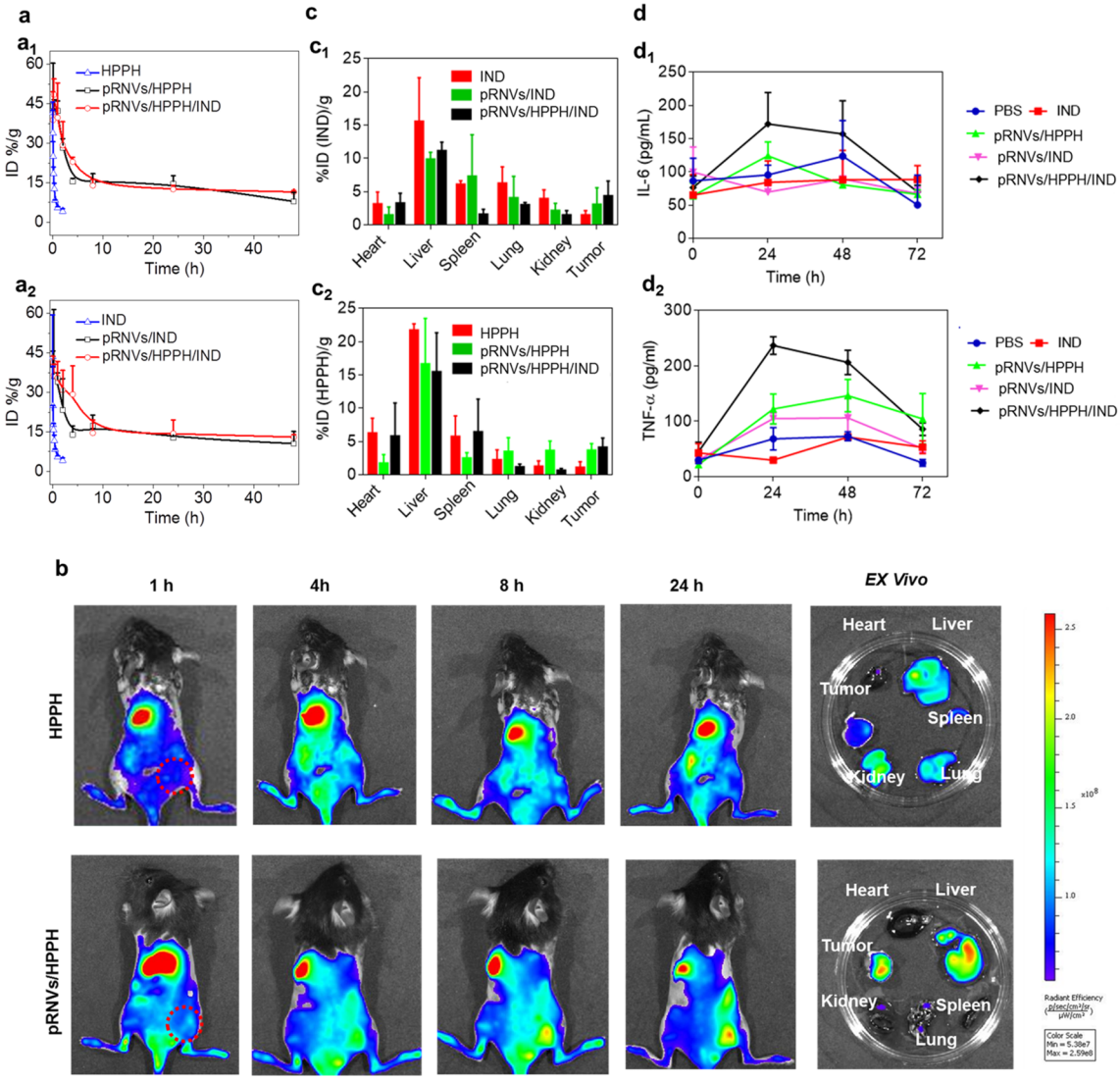

Figure 5. (a_1, a_2) **Pharmacokinetics of HPPH and IND formulations in C57BL/6 mice at different time points. (b) NIR fluorescence imaging of HPPH and pRNVs/HPPH after *i.v.* injection in MC38-tumor bearing C57BL/6 mice. (c_1, c_2) IND and HPPH biodistribution at 8 h after intravenous injection in B16F10-tumor bearing C57BL/6 mice. (d) Blood IL-6 and TNF-α levels in B16F10 tumor-bearing C57BL/6 mice after each drug formulation treatment. Mice with HPPH formulation injection received laser irradiation at 671 nm (200 mW/cm^2, 10 min). Data are represented as the mean ± SD (n = 3/group).**

the material function as both nanocarrier and therapeutic agent to directly activate host's immune response.

We then investigated the possible mechanism for the specific ICD of pRNVs in B16F10 cells. ICD effect *via* CRT exposure can be translocation of CRT from endoplasmic reticulum (ER) or nuclei to cell membrane.[14] We hypothesize that pRNVs can specifically target ER in B16F10 cells causing CRT exposure. We also hypothesize that CRT levels are different in different types of cancer cells. We thus investigated the subcellular distribution of pRNVs. From Figure S12, Cy5-labeled pRNVs (Cy5-pRNVs) mainly localized in ER of B16F10 cells after internalization, with a negligible amount trapped in endo/lysosome or mitochondria. On the other hand, Cy5-labeled NVs (Cy5-NVs) distributed in both ER and endo/lysosome. According to Figure S17a, pRNVs can target to ER in B16F10, MC38, and 4T1. Results from Figure S17b revealed that CRT level in B16F10 cells is much higher than that in the other two cell types. Therefore, B16F10 cells are more sensitive to pRNVs for ICD effect.

ICD Effect of pRNVs/HPPH/IND Mediated Both by pRNVs and PDT in B16F10 Cells. We then investigated the ICD effect of pRNVs/HPPH/IND in B16F10 cells mediated by both pRNVs and PDT *via* CLSM and flow cytometry. As shown in Figure 4a, significant green Alexa-488 CRT fluorescence was observed for CRT exposure in B16F10 cells after different HPPH formulations treatment with laser irradiation. pRNVs alone and pRNVs/IND also induced ICD as Alexa-488 CRT was observed. IND alone did not elicit any ICD effect on B16F10 cells. According to Figure S18 without laser irradiation, HPPH formulations also displayed weak ICD effect as demonstrated by the green fluorescence observed, which is once again attributed to dark toxicity. Flow cytometry results in Figure 4b also confirmed the similar phenomena that HPPH formulation with laser irradiation and pRNVs alone could induce ICD based on the intensity shift in the fluorescence spectra.

Cell Apoptosis Investigation. To better understand the relationship between cell death and PDT/ICD, we assessed

DOI: 10.1021/acsnano.9b07212
ACS Nano 2020, 14, 620−631

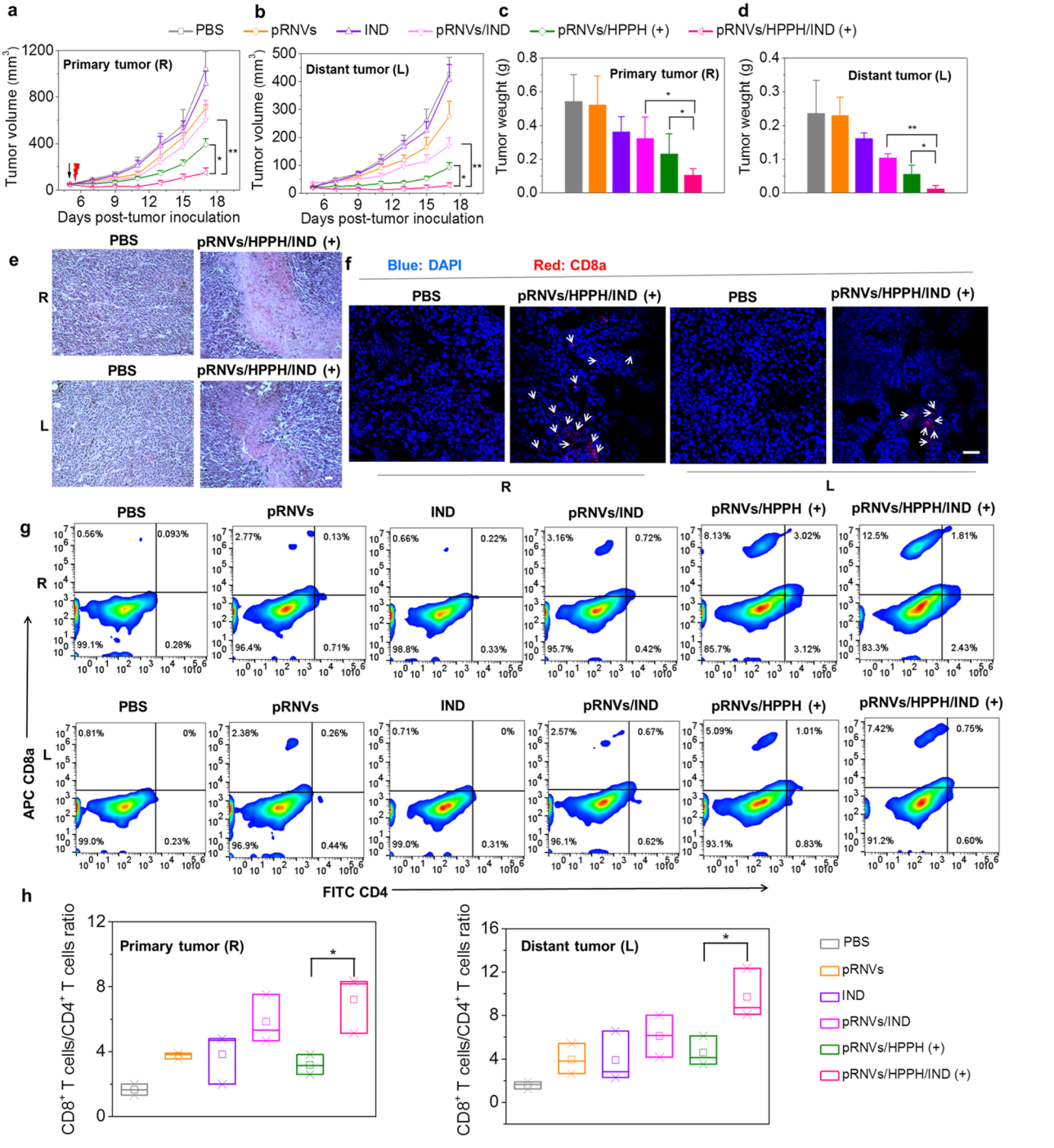

Figure 6. Antitumor efficacy of pRNVs, IND, pRNVs/IND, pRNVs/HPPH, and pRNVs/HPPH/IND on C57BL/6 mice bearing B16F10 tumor for primary (a) and distant tumors (b) within 17 d post-tumor inoculation (n = 5). (c, d) Primary and distant tumors weight after treatment by different formulations at 17 d. (Statistical analysis: one-way ANOVA with Tukey's multiple comparisons. *$p < 0.05$, **$p < 0.01$). (e) Hematoxylin and eosin (H & E) staining for primary and distant tumor section. (f) $CD8^+$ T cells distribution in primary and distant tumor tissues for mice treated by pRNVs/HPPH/IND (+) by CLSM characterization. PBS group acted as a control. White arrows showed the location of $CD8^+$ T cells. (g) $CD8^+$ and $CD4^+$ T cell infiltration and (h) ratio of $CD8^+$ and $CD4^+$ T cells in both primary and distant tumors for mice after different formulation treatment. Symbol (+) means pRNVs/HPPH and pRNVs/HPPH/IND treated mice acquired laser irradiation (671 nm, 200 mW/cm^2, 10 min) after 24 h injection. Scale bar 40 μm. Data are presented as the mean ± SD.

cell apoptosis after treatment. According to Figure 4c, pRNVs induced preapoptosis with little apoptosis (13.2%) observed in B16F10 cells, which probably caused ICD by preapoptotic exposure of CRT. IND scarcely caused cell death (11.6%). With laser irradiation, free HPPH (39.4%) and HPPH/IND (36.4%) caused early apoptosis. Both early apoptosis and late apoptosis were observed in B16F10 cells treated by pRNVs/HPPH (20.6%, 33.6%) and pRNVs/HPPH/IND (10.1%, 45.6%) after laser treatment (671 nm, 100 mW/cm^2, 1 min). The addition of IND caused the B16F10 cells to undergo more late stage apoptosis for pRNVs/HPPH/IND (45.6%) compared to pRNVs/HPPH (33.6%).

DOI: 10.1021/acsnano.9b07212
ACS Nano 2020, 14, 620−631

Pharmacokinetic Profile, NIR Fluorescence Imaging, Drug Biodistribution, and Cytokine Secretion Investigation. Prolonged blood circulation is important for EPR effect and tumor accumulation of drug nanoformulations. According to Figure 5a$_1$,a$_2$, both HPPH ($t_{1/2\alpha}$, pNRV/HPPH (3.02 h), pNRV/HPPH/IND (2.52 h)) and IND ($t_{1/2\alpha}$, pNRV/IND (2.67 h), pNRV/HPPH/IND (3.12 h)) nanoformulations displayed much longer retention in the blood over free HPPH ($t_{1/2\alpha}$, HPPH (0.23 h) and IND (0.19 h). Then we studied whether the nanosystem could have good tumor accumulation by using the MC38 tumor model and pNRV/HPPH nanoformula as an example. As shown in Figure 5b, pNRV/HPPH revealed apparent tumor accumulation at 8 h post injection and even higher fluorescence intensity at 24 h. As to free drug treated mice, little to no tumor accumulation was observed. The *ex vivo* results also confirmed the observation. From drug biodistribution results in Figure 5c, nanoformulas treated mice also indicated higher tumor uptake than free drugs. Both the weak adjuvant function of pRNVs and released danger signals from ICD/PDT could promote DC maturation and pro-inflammation secretion. Then we tested the IL-6 and TNF-α levels in blood for mice treated with different formulas. As shown in Figure 5d, cytokine (e.g., IL-6, TNF-α) concentrations were the highest for mice that underwent pNRV/HPPH/IND treatment with laser irradiation at 24 and 48 h post injection.

Significant *in Vivo* Antitumor Efficacy and Abscopal Effect of pRNVs/HPPH/IND. To assess the antitumor efficacy of pRNVs/HPPH/IND, C57BL/6 female mice (6−8 weeks, 18−20 g) were subcutaneously inoculated 5×10^5 B16F10 cells at right flank (primary tumor) and 1×10^5 cells at left side (distant tumor) per mouse. At 5 d post tumor inoculation when primary tumor size reached 100 mm^3, mice were randomly divided into six groups (n = 5) and treated by PBS, pRNVs, IND, pRNVs/IND, pRNVs/HPPH, and pRNVs/HPPH/IND *via* intravenous (*i.v.*) injection (pRNVs: 5 mg/kg, HPPH: 0.15 mg/kg, IND: 0.5 mg/kg). After 24 h injection, mice treated with pRNVs/HPPH and pRNVs/HPPH/IND received laser irradiation (671 nm, 200 mW/cm^2, 10 min).

Due to the ICD effect, single pRNVs indicated weak primary and distant tumor inhibition efficacy from Figure 6a,b. In combination with IND, pRNVs/IND showed similar primary antitumor efficacy with pRNVs (Figure 6a,b). However, pRNVs/IND could better suppress distant tumor growth than pRNVs alone, possibly because the smaller distant tumor was more sensitive to tumor microenvironment modulation than the primary tumor. Moreover, pRNVs/HPPH could significantly inhibit both primary and distant tumor growth within 17 d post tumor inoculation (Figure 6a,b). Nevertheless, due to the immunosuppressive factor (e.g., IDO), more T_{regs} were present, which in turn weakened CD8$^+$ T cell activation. Tumors for mice treated with pRNVs/HPPH displayed distinct rebound from 13 to 17 d after tumor inoculation for the above reason. In addition, when combined with low dose IND, pRNVs/HPPH/IND significantly reduced tumor growth and alleviated immunosuppressive effects by reinvigorating CD8$^+$ T cells (Figure 6a,b). Meantime, free IND hardly suppressed tumor growth and was similar to the PBS group. According to Figure S10, negligible body weight changes were observed indicating the good biocompatibility of the nanoplatform. Images demonstrated noticeable tumor shrinkage for mice after pRNVs/HPPH/IND treatment (Figure S11), along with having the lowest gross tumor weights for primary and distant tumor compared with the other groups (Figure 6c,d). Apparent tumor cells death for mice treated with pRNVs/HPPH/IND were observed from H & E staining (Figure 6e). Tumors for mice treated by pRNVs, pRNVs/IND and pRNVs/HPPH also revealed cell death (Figure S12). No normal organ damage was observed in the treated mice, demonstrating good safety profile of the nanoplatform (Figure S13).

Tumor-Infiltrating Lymphocyte Distribution. We then investigated whether tumor shrinkage was correlated with CD8$^+$ T cells infiltration. Due to the ICD effect of pRNVs alone, pRNVs and pRNVs/IND could also provoke immune response and facilitate CD8$^+$ T cells permeation (Red fluorescence) (Figure S14). pRNVs/HPPH with laser irradiation (671 nm, 200 mW/cm^2, 10 min) promoted more CD8$^+$ T cells (Red fluorescence) distribution in tumor tissues (Figure S14). With IND addition, pRNVs/HPPH/IND with laser irradiation (671 nm, 200 mW/cm^2, 10 min) significantly led to higher CD8$^+$ T cells activation (Figure 5f and Figure S14). According to the flow cytometry results (Figure 6g), pRNVs/HPPH/IND treatment with laser irradiation (671 nm, 200 mW/cm^2, 10 min) caused the most CD8$^+$ T cell infiltration in both primary and distant tumor tissues compared with other groups. In addition, pRNVs/HPPH/IND with laser irradiation also caused higher ratio of CD8$^+$ T cells and CD4$^+$ T cells in tumors compared with just pRNVs/HPPH treatment indicating that IND addition could reverse tumor microenvironment and reinvigorate CD8$^+$ T cells.

CONCLUSIONS

In summary, we constructed a smart nanovesicle platform (pRNVs/HPPH/IND) for effective B16F10 cancer immunotherapy. pRNVs not only acted as a nanocarrier encapsulating both HPPH and IND but also had ICD effect especially on B16F10 cells. The relatively fast internalization and endo/lysosomal escape of pRNVs/HPPH as well as efficient drug delivery allowed us to induce severe cytotoxicity due to ROS generation with laser irradiation and ICD effect. With laser irradiation, pRNVs/HPPH/IND caused significant cell apoptosis (55.7%) in B16F10 cells. Due to the ICD from both pRNVs and HPPH, PDT mediated by HPPH, and TME modulation *via* IND for activation of P-S6K, pRNVs/HPPH/IND significantly inhibited both primary and distant B16F10 tumors. Notably, there was an increase in CD8$^+$ T cell infiltration at both tumor sites. The smart nanovesicles platform highlights the importance of rational design of nanomaterials to achieve potent cancer immunotherapy.

METHODS

Synthesis of PEG-*b*-PPT. The PEG-*b*-PPT was synthesized using ring-opening polymerization of the alkynyl NCA monomer. Briefly, mPEG-NH$_2$ (5 kDa, 250 mg, 1 equiv) and alkynyl NCA monomer (264 mg, 25 equiv) was mixed in 10 mL of anhydrous DMF at room temperature. The flask was under continuous nitrogen flow to facilitate polymerization. ^{1}H NMR was used to monitor the polymerization and more than 99% monomer was consumed in 20 h. The polymer was purified by three times precipitation from DMF into diethyl ether to afford a pale yellow powder after drying in vacuum (348 mg, yield: 68%)

Synthesis of PEG-*b*-cPPT. Cationic polymer PEG-*b*-cPPT was obtained by postpolymerization modification of block copolymer PEG$_{113}$-b-PPT$_{25}$ with 2-diethylaminoethanethiol hydrochloride *via* thiol−yne click reactions. Briefly, PEG$_{113}$-*b*-PPT$_{25}$ (119 mg, 1 eq), DMPA (63 mg, 12.5 equiv), and 2-diethylaminoethanethiol hydro-

DOI: 10.1021/acsnano.9b07212
ACS Nano 2020, 14, 620−631

chloride (840 mg, 375 equiv) were added into 20 mL of anhydrous DMF in a 100 mL flask. The reaction mixture was then bubbled with nitrogen for 10 min and placed under UV light with a wavelength of 365 nm for 2 h. The mixture was transferred into a presoaked dialysis membrane tubing (MWCO 6−8 kDa), dialyzed against nanopure water for another 2 days, and lyophilized to obtain the final product (153 mg, yield: 66%)

Preparation of pH-Responsive Nanovesicles (pRNVs) and Drug Loading To form pRNVs/HPPH/IND. pRNVs were acquired *via* solvent exchange method. In brief, copolymer PEG-*b*-cPPT solution in methanol (10 mg/mL, 50 μL) was added dropwise to 950 μL phosphate buffer saline (PBS, 10 mM, pH 7.4, 150 mM NaCl). The mixture was allowed to stand for 20 min before agitation by rotation. After volatilization in a drought cupboard and dialysis (MWCO, 3500) in PBS (10 mM, pH 7.4, 150 mM NaCl) to remove methanol, the pRNVs were prepared. The size, size distribution, and zeta potential were measured by DLS. Nanovesicles (NVs) self-assembled from the other control copolymer (PEG-*b*-PPT) were obtained by the similar methods. HPPH and IND loaded pRNVs (pRNVs/HPPH/IND) were prepared according to listed methods above. In short, HPPH (5 mg/mL, 1.5 μL) solution in DMSO and IND (0.1 mg/mL, 0.25 mL) in methanol was mixed with PEG-*b*-cPPT copolymer solution (10 mg/mL, 50 μL) in methanol. The mixtures were slowly added to 950 μL of PBS (10 mM, pH 7.4, 150 mM NaCl) buffer from the bottom. The mixture was allowed to stand for 20 min before agitation by rotation. After volatilization in drought cupboard and dialysis in PBS buffer, pRNVs/HPPH/IND was obtained.

Cytotoxicity of pRNVs/HPPH/IND in B16F10 Cells. The cytotoxicity of pRNVs/HPPH/IND in B16F10 cells was characterized by MTT assays. In brief, 5.0×10^3 cells were seeded in 96-well plates supplemented with Dulbecco's modified eagle media (DMEM) containing 10% fetal bovine serum (FBS), 1% penicillin, and streptomycin (37 °C, 5% CO_2). After 24 h, free HPPH, IND, HPPH/IND, pRNVs, pRNVs/HPPH, pRNVs/IND, and pRNVs/HPPH/IND were separately added (n = 8). After 24 h incubation, all of the media were aspirated and replenished with fresh media. Half cells (n = 4) treated by different formulations got laser irradiation at 671 nm (100 mW/cm^2, 1 min). After another 24 h, 10 μL of MTT (5 mg/mL) was added for 4 h incubation, and all of the media and MTT were aspirated, replaced by 150 μL DMSO. After mixing several minutes, the absorbance was acquired by a BioTek Synergy H4 hybrid reader at 570 nm.

IDO Activity Test by Western Blot. IDO activity in B16F10 cells was tested by Western blot. We first tested the IDO expression in B16F10 cells after different IFN-γ stimulation. Briefly, 1.0×10^6 cells per well were seeded in 6-well plates supplemented with DMEM media with 10% FBS, 1% penicillin, and streptomycin. After 24 h, IFN-γ (concentration from low to high: 0, 50, 100, 200 ng/mL) was added to each well for another 24 h incubation. Then the IDO expression was tested by Western blot. At first, cells in each well were lysed with 100 μL of RIPA buffer containing 10% cocktail inhibitor for 30 min on ice. After centrifugation for 15 min (4 °C, 12000 rpm), protein in supernatant was isolated. Protein concentration in cells treated by each sample was quantified by a BCA kit. Equal protein mass was added to each well in NuPAGE 10% Bis-tris-gel with running buffer covered for 90 min. After electrophoresis, proteins were transferred from gel to membrane in transfer buffer for another 80 min. After initial blocking in 3% BSA for 1 h, membrane was stained by primary antibody (overnight at 4 °C). After three washes with PBST, the membrane was stained by secondary antibody for 1 h at rt. After washing three timeswith PBST buffer, chemiluminescent substrate was added to the membrane, which was exposed in Amersham Imager 600 to obtain the images.

We then investigated whether IND formulations could inhibit IDO expression or up-regulation P-S6K1. In brief, 1.0×10^6 cells per well were seeded in 6-well plates and different IND formulations (IND concentration: 25 μg/mL) with 100 ng/mL IFN-γ were added to each well for 24 h culture. After another 24 h incubation, IDO expression and P-S6K1 were tested by Western blot.

ICD Induced by Nanocarrier pRNVs in Different Cancer Cells. We detected whether NVs and pRNVs had an ICD effect on B16F10, MC38, and 4T1 cells *via* CRT exposure by flow cytometry. In brief, 5.0×10^5 B16F10, MC38 cells with DMEM media containing 10% FBS, 1% penicillin, and streptomycin and 4T1 cells with RPMI-1640 media containing 10% FBS, 1% penicillin, and streptomycin were separately seeded in 6-well plates. After 24 h, NVs and pRNVs (n = 2) were added to each well for another 24 h. One well in each group received laser irradiation at 671 nm (100 mW/cm^2, 1 min). After 4 h, cells were digested by trypsin, centrifuged, and washed by PBS. Then cells were stained with Alexa Flour 647-CRT for 40 min at rt, washed by PBS (× 3), suspended in 0.5 mL of PBS, and tested by flow cytometry.

ICD Effect of pRNVs/HPPH/IND on B16F10 Cells. We mainly tested the CRT exposure of B16F10 cells to determine the ICD effect after cells treated by different formulations *via* CLSM. In short, 2.0×10^4 B16F10 cells were seeded in 8-well plate incubation for 24 h. Then pRNVs, free HPPH, free IND, free HPPH/IND, pRNVs/HPPH, pRNVs/IND, and pRNVs/HPPH/IND (n = 2) were added separately. After 24 h, one well of each group was irradiated with 671 nm (100 mW/cm^2, 1 min). After another 4 h incubation, the media were aspirated and cells were washed by PBS, fixed with Z-fix solution, stained with Anti Alexa Fluor 488-CRT, covered with mounting media with DAPI, and sealed with nail polish. The images were acquired by CLSM.

Cell Apoptosis Induced by pRNVs/HPPH/IND. Cell apoptosis mediated by pRNVs/HPPH/IND was characterized with an Annex V/PI kit. In short, 5.0×10^5 B16F10 cells with DMEM media containing 10% FBS, 1% penicillin, and streptomycin were seeded in 6-well plates. pRNVs, free HPPH, free IND, free HPPH/IND, pRNVs/HPPH, pRNVs/IND, and pRNVs/HPPH/IND were added to each well for 24 h. After another 24 h incubation, cells treated by HPPH formulations received laser irradiation at 671 nm (100 mW/cm^2, 1 min). After another 4 h incubation, cell supernatant was collected and cells were digested, centrifuged, and washed by PBS. After that, cells were stained with Annex V/PI according to the manufacturer's protocol. Following centrifugation and washing by PBS, cells were finally suspended in binding buffer and tested by flow cytometry.

ASSOCIATED CONTENT

Supporting Information

The Supporting Information is available free of charge at https://pubs.acs.org/doi/10.1021/acsnano.9b07212.

Materials, characterization, synthesis of *N*-carboxyanhydride (NCA) monomer, *in vitro* drug release, cellular uptake of pNRV/HPPH/IND and endo/lysosomal escape, ROS generation for PDT, cellular uptake of NVs/HPPH and pRNVs/HPPH in different cell lines, ICD effect of pRNVs/HPPH/IND on B16F10 cells, TIL infiltration (PDF)

AUTHOR INFORMATION

Corresponding Authors

*Email: hushuo_xy@163.com.
*Email: shawn.chen@nih.gov.

ORCID

Fuwu Zhang: 0000-0002-1928-3472
Hongzhang Deng: 0000-0003-3637-8905
Sheng Wang: 0000-0002-4797-5310
Xiaoyuan Chen: 0000-0002-9622-0870

Author Contributions

‖W.Y. and F.Z. contributed equally to this work.

Notes

The authors declare no competing financial interest.

DOI: 10.1021/acsnano.9b07212
ACS Nano 2020, 14, 620−631

ACKNOWLEDGMENTS

This work was supported by the Intramural Research Program (IRP) of the National Institute of Biomedical Imaging and Bioengineering (NIBIB), National Institutes of Health (NIH), and National Natural Science Foundation of China (NSFC 81471689, 81771873 and 91859207). All animal experiments were performed under a National Institutes of Health Animal Care and Use Committee (NIH ACUC) approved protocol. We thank Dr. Vincent Schram at the NICHD Microscopy Imaging Core for technical support.

REFERENCES

(1) Mellman, I.; Coukos, G.; Dranoff, G. Cancer Immunotherapy Comes of Age. *Nature* **2011**, *480*, 480−489.
(2) Drake, C. G.; Lipson, E. J.; Brahmer, J. R. Breathing New Life Into Immunotherapy: Review of Melanoma, Lung and Kidney Cancer. *Nat. Rev. Clin. Oncol.* **2014**, *11*, 24−37.
(3) Melero, I.; Gaudernack, G.; Gerritsen, W.; Huber, C.; Parmiani, G.; Scholl, S.; Thatcher, N.; Wagstaff, J.; Zielinski, C.; Faulkner, I.; Mellstedt, H. Therapeutic Vaccines for Cancer: An Overview of Clinical Trials. *Nat. Rev. Clin. Oncol.* **2014**, *11*, 509−524.
(4) Yang, X.; Zhao, J.; Duan, S.; Hou, X.; Li, X.; Hu, Z.; Tang, Z.; Mo, F.; Lu, X. Enhanced Cytotoxic T Lymphocytes Recruitment Targeting Tumor Vasculatures by Endoglin Aptamer and IP-10 Plasmid Presenting Liposome-Based Nanocarriers. *Theranostics* **2019**, *9*, 4066−4083.
(5) Pardoll, D. M. The Blockade of Immune Checkpoints in Cancer Immunotherapy. *Nat. Rev. Cancer* **2012**, *12*, 252−264.
(6) Riley, R. S.; June, C. H.; Langer, R.; Mitchell, M. J. Delivery Technologies for Cancer Immunotherapy. *Nat. Rev. Drug Discovery* **2019**, *18*, 175−196.
(7) Nam, J.; Son, S.; Park, K. S.; Zou, W.; Shea, L. D.; Moon, J. J. Cancer Nanomedicine for Combination Cancer Immunotherapy. *Nat. Rev. Mater.* **2019**, *4*, 398−414.
(8) Shi, Y.; Lammers, T. Combining Nanomedicine and Immunotherapy. *Acc. Chem. Res.* **2019**, *52*, 1543−1554.
(9) Yang, W.; Zhou, Z.; Lau, J.; Hu, S.; Chen, X. Functional T Cell Activation by Smart Nanosystems for Effective Cancer Immunotherapy. *Nano Today* **2019**, *27*, 28−47.
(10) Chen, Z.; Wang, Z.; Gu, Z. Bioinspired and Biomimetic Nanomedicines. *Acc. Chem. Res.* **2019**, *52*, 1255−1264.
(11) Lee, E. S.; Shin, J. M.; Son, S.; Ko, H.; Um, W.; Song, S. H.; Lee, J. A.; Park, J. H. Recent Advances in Polymeric Nanomedicines for Cancer Immunotherapy. *Adv. Healthcare Mater.* **2019**, *8*, 1801320.
(12) Galluzzi, L.; Buque, A.; Kepp, O.; Zitvogel, L.; Kroemer, G. Immunogenic Cell Death in Cancer and Infectious Disease. *Nat. Rev. Immunol.* **2017**, *17*, 97−111.
(13) Obeid, M.; Tesniere, A.; Ghiringhelli, F.; Fimia, G. M.; Apetoh, L.; Perfettini, J. L.; Castedo, M.; Mignot, G.; Panaretakis, T.; Casares, N.; Metivier, D.; Larochette, N.; van Endert, P.; Ciccosanti, F.; Piacentini, M.; Zitvogel, L.; Kroemer, G. Calreticulin Exposure Dictates the Immunogenicity of Cancer Cell Death. *Nat. Med.* **2007**, *13*, 54−61.
(14) Krysko, D. V.; Garg, A. D.; Kaczmarek, A.; Krysko, O.; Agostinis, P.; Vandenabeele, P. Immunogenic Cell Death and DAMPs in Cancer Therapy. *Nat. Rev. Cancer* **2012**, *12*, 860−875.
(15) Lu, K.; He, C.; Guo, N.; Chan, C.; Ni, K.; Lan, G.; Tang, H.; Pelizzari, C.; Fu, Y. X.; Spiotto, M. T.; Weichselbaum, R. R.; Lin, W. Low-Dose X-ray Radiotherapy-Radiodynamic Therapy *via* Nanoscale Metal-Organic Frameworks Enhances Checkpoint Blockade Immunotherapy. *Nat. Biomed. Eng.* **2018**, *2*, 600−610.
(16) Yang, W.; Zhu, G.; Wang, S.; Yu, G.; Yang, Z.; Lin, L.; Zhou, Z.; Liu, Y.; Dai, Y.; Zhang, F.; Shen, Z.; Liu, Y.; He, Z.; Lau, J.; Niu, G.; Kiesewetter, D. O.; Hu, S.; Chen, X. *In Situ* Dendritic Cell Vaccine for Effective Cancer Immunotherapy. *ACS Nano* **2019**, *13*, 3083−3094.
(17) Song, W.; Shen, L.; Wang, Y.; Liu, Q.; Goodwin, T. J.; Li, J.; Dorosheva, O.; Liu, T.; Liu, R.; Huang, L. Synergistic and Low Adverse Effect Cancer Immunotherapy by Immunogenic Chemotherapy and Locally Expressed PD-L1 Trap. *Nat. Commun.* **2018**, *9*, 2237.
(18) Barker, H. E.; Paget, J. T.; Khan, A. A.; Harrington, K. J. The Tumour Microenvironment After Radiotherapy: Mechanisms of Resistance and Recurrence. *Nat. Rev. Cancer* **2015**, *15*, 409−425.
(19) Duan, X.; Chan, C.; Lin, W. Nanoparticle-Mediated Immunogenic Cell Death Enables and Potentiates Cancer Immunotherapy. *Angew. Chem., Int. Ed.* **2019**, *58*, 670−680.
(20) He, C.; Duan, X.; Guo, N.; Chan, C.; Poon, C.; Weichselbaum, R. R.; Lin, W. Core-Shell Nanoscale Coordination Polymers Combine Chemotherapy and Photodynamic Therapy to Potentiate Checkpoint Blockade Cancer Immunotherapy. *Nat. Commun.* **2016**, *7*, 12499.
(21) Yang, B.; Chen, Y.; Shi, J. Reactive Oxygen Species (ROS)-Based Nanomedicine. *Chem. Rev.* **2019**, *119*, 4881−4985.
(22) Castano, A. P.; Mroz, P.; Hamblin, M. R. Photodynamic Therapy and Anti-Tumour Immunity. *Nat. Rev. Cancer* **2006**, *6*, 535−545.
(23) Li, X.; Kwon, N.; Guo, T.; Liu, Z.; Yoon, J. Innovative Strategies for Hypoxic-Tumor Photodynamic Therapy. *Angew. Chem., Int. Ed.* **2018**, *57*, 11522−11531.
(24) Jiang, Y.; Li, J.; Zeng, Z.; Xie, C.; Lyu, Y.; Pu, K. Organic Photodynamic Nanoinhibitor for Synergistic Cancer Therapy. *Angew. Chem., Int. Ed.* **2019**, *58*, 8161−8165.
(25) Lovell, J. F.; Liu, T. W. B.; Chen, J.; Zheng, G. Activatable Photosensitizers for Imaging and Therapy. *Chem. Rev.* **2010**, *110*, 2839−2857.
(26) Yu, G.; Cen, T. Y.; He, Z.; Wang, S. P.; Wang, Z.; Ying, X. W.; Li, S.; Jacobson, O.; Wang, S.; Wang, L.; Lin, L. S.; Tian, R.; Zhou, Z.; Ni, Q.; Li, X.; Chen, X. Porphyrin Nanocage-Embedded Single-Molecular Nanoparticles for Cancer Nanotheranostics. *Angew. Chem., Int. Ed.* **2019**, *58*, 8799.
(27) Mao, C.; Li, F.; Zhao, Y.; Debinski, W.; Ming, X. P-Glycoprotein-Targeted Photodynamic Therapy Boosts Cancer Nanomedicine by Priming Tumor Microenvironment. *Theranostics* **2018**, *8*, 6274−6290.
(28) Luby, B. M.; Walsh, C. D.; Zheng, G. Advanced Photosensitizer Activation Strategies for Smarter Photodynamic Therapy Beacons. *Angew. Chem., Int. Ed.* **2019**, *58*, 2558−2569.
(29) Zhang, F.; Ni, Q.; Jacobson, O.; Cheng, S.; Liao, A.; Wang, Z.; He, Z.; Yu, G.; Song, J.; Ma, Y.; Niu, G.; Zhang, L.; Zhu, G.; Chen, X. Polymeric Nanoparticles with a Glutathione-Sensitive Heterodimeric Multifunctional Prodrug for *In Vivo* Drug Monitoring and Synergistic Cancer Therapy. *Angew. Chem., Int. Ed.* **2018**, *57*, 7066−7070.
(30) Li, J.; Huang, J.; Lyu, Y.; Huang, J.; Jiang, Y.; Xie, C.; Pu, K. Photoactivatable Organic Semiconducting Pro-Nanoenzymes. *J. Am. Chem. Soc.* **2019**, *141*, 4073−4079.
(31) Ou, W.; Jiang, L.; Thapa, R. K.; Soe, Z. C.; Poudel, K.; Chang, J. H.; Ku, S. K.; Choi, H. G.; Yong, C. S.; Kim, J. O. Combination of NIR Therapy and Regulatory T Cell Modulation Using Layer-by-Layer Hybrid Nanoparticles for Effective Cancer Photoimmunotherapy. *Theranostics* **2018**, *8*, 4574−4590.
(32) Wang, H.; Han, X.; Dong, Z.; Xu, J.; Wang, J.; Liu, Z. Hyaluronidase with pH-Responsive Dextran Modification as an Adjuvant Nanomedicine for Enhanced Photodynamic-Immunotherapy of Cancer. *Adv. Funct. Mater.* **2019**, *29*, 1902440.
(33) Chen, Z.; Liu, L.; Liang, R.; Luo, Z.; He, H.; Wu, Z.; Tian, H.; Zheng, M.; Ma, Y.; Cai, L. Bioinspired Hybrid Protein Oxygen Nanocarrier Amplified Photodynamic Therapy for Eliciting Anti-Tumor Immunity and Abscopal Effect. *ACS Nano* **2018**, *12*, 8633−8645.
(34) Meng, Z.; Zhou, X.; Xu, J.; Han, X.; Dong, Z.; Wang, H.; Zhang, Y.; She, J.; Xu, L.; Wang, C.; Liu, Z. Light-Triggered *In Situ* Gelation to Enable Robust Photodynamic-Immunotherapy by Repeated Stimulations. *Adv. Mater.* **2019**, *31*, 1900927.

DOI: 10.1021/acsnano.9b07212
ACS Nano 2020, 14, 620−631

(35) Ng, C. W.; Li, J.; Pu, K. Recent Progresses in Phototherapy-Synergized Cancer Immunotherapy. *Adv. Funct. Mater.* **2018**, *28*, 1804688.
(36) Liu, W. L.; Zou, M. Z.; Liu, T.; Zeng, J. Y.; Li, X.; Yu, W. Y.; Li, C. X.; Ye, J. J.; Song, W.; Feng, J.; Zhang, X. Z. Expandable Immunotherapeutic Nanoplatforms Engineered from Cytomembranes of Hybrid Cells Derived from Cancer and Dendritic Cells. *Adv. Mater.* **2019**, *31*, 1900499.
(37) Phuengkham, H.; Ren, L.; Shin, I. W.; Lim, Y. T. Nanoengineered Immune Niches for Reprogramming the Immunosuppressive Tumor Microenvironment and Enhancing Cancer Immunotherapy. *Adv. Mater.* **2019**, *31*, 1803322.
(38) Gao, S.; Yang, D.; Fang, Y.; Lin, X.; Jin, X.; Wang, Q.; Wang, X.; Ke, L.; Shi, K. Engineering Nanoparticles for Targeted Remodeling of the Tumor Microenvironment to Improve Cancer Immunotherapy. *Theranostics* **2019**, *9*, 126−151.
(39) Liu, J.; Chen, Q.; Feng, L.; Liu, Z. Nanomedicine for Tumor Microenvironment Modulation and Cancer Treatment Enhancement. *Nano Today* **2018**, *21*, 55−73.
(40) Hou, L.; Liu, Q.; Shen, L.; Liu, Y.; Zhang, X.; Chen, F.; Huang, L. Nano-Delivery of Fraxinellone Remodels Tumor Microenvironment and Facilitates Therapeutic Vaccination in Desmoplastic Melanoma. *Theranostics* **2018**, *8*, 3781−3796.
(41) Musetti, S.; Huang, L. Nanoparticle-Mediated Remodeling of the Tumor Microenvironment to Enhance Immunotherapy. *ACS Nano* **2018**, *12*, 11740−11755.
(42) Lu, J.; Liu, X.; Liao, Y. P.; Salazar, F.; Sun, B.; Jiang, W.; Chang, C. H.; Jiang, J.; Wang, X.; Wu, A. M.; Meng, H.; Nel, A. E. Nano-Enabled Pancreas Cancer Immunotherapy Using Immunogenic Cell Death and Reversing Immunosuppression. *Nat. Commun.* **2017**, *8*, 1811.
(43) Zhang, X.; Wang, C.; Wang, J.; Hu, Q.; Langworthy, B.; Ye, Y.; Sun, W.; Lin, J.; Wang, T.; Fine, J.; Cheng, H.; Dotti, G.; Huang, P.; Gu, Z. PD-1 Blockade Cellular Vesicles for Cancer Immunotherapy. *Adv. Mater.* **2018**, *30*, 1707112.
(44) Cheng, K.; Ding, Y.; Zhao, Y.; Ye, S.; Zhao, X.; Zhang, Y.; Ji, T.; Wu, H.; Wang, B.; Anderson, G. J.; Ren, L.; Nie, G. Sequentially Responsive Therapeutic Peptide Assembling Nanoparticles for Dual-Targeted Cancer Immunotherapy. *Nano Lett.* **2018**, *18*, 3250−3258.
(45) Li, J.; Cui, D.; Huang, J.; He, S.; Yang, Z.; Zhang, Y.; Luo, Y.; Pu, K. Organic Semiconducting Pro-Nanostimulants for Near-Infrared Photoactivatable Cancer Immunotherapy. *Angew. Chem., Int. Ed.* **2019**, *58*, 12680−12687.
(46) Katz, J. B.; Muller, A. J.; Prendergast, G. C. Indoleamine 2,3-Dioxygenase in T-Cell Tolerance and Tumoral Immune Escape. *Immunol. Rev.* **2008**, *222*, 206−221.
(47) Munn, D. H.; Mellor, A. L. Indoleamine 2,3-Dioxygenase and Metabolic Control of Immune Responses. *Trends Immunol.* **2013**, *34*, 137−143.
(48) Munn, D. H.; Mellor, A. L. IDO in the Tumor Microenvironment: Inflammation, Counter-Regulation, and Tolerance. *Trends Immunol.* **2016**, *37*, 193−207.
(49) Wang, N.; Wang, Z.; Xu, Z.; Chen, X.; Zhu, G. A Cisplatin-Loaded Immunochemotherapeutic Nanohybrid Bearing Immune Checkpoint Inhibitors for Enhanced Cervical Cancer Therapy. *Angew. Chem., Int. Ed.* **2018**, *57*, 3426−3430.
(50) Peng, J.; Xiao, Y.; Li, W.; Yang, Q.; Tan, L.; Jia, Y.; Qu, Y.; Qian, Z. Photosensitizer Micelles Together with IDO Inhibitor Enhance Cancer Photothermal Therapy and Immunotherapy. *Adv. Sci.* **2018**, *5*, 1700891.
(51) Lu, J.; Liu, X.; Liao, Y. P.; Wang, X.; Ahmed, A.; Jiang, W.; Ji, Y.; Meng, H.; Nel, A. E. Breast Cancer Chemo-Immunotherapy Through Liposomal Delivery of an Immunogenic Cell Death Stimulus Plus Interference in the IDO-1 Pathway. *ACS Nano* **2018**, *12*, 11041−11061.
(52) Zhu, G.; Mei, L.; Vishwasrao, H. D.; Jacobson, O.; Wang, Z.; Liu, Y.; Yung, B. C.; Fu, X.; Jin, A.; Niu, G.; Wang, Q.; Zhang, F.; Shroff, H.; Chen, X. Intertwining DNA-RNA Nanocapsules Loaded with Tumor Neoantigens as Synergistic Nanovaccines for Cancer Immunotherapy. *Nat. Commun.* **2017**, *8*, 1482.
(53) Ni, Q.; Zhang, F.; Zhang, Y.; Zhu, G.; Wang, Z.; Teng, Z.; Wang, C.; Yung, B. C.; Niu, G.; Lu, G.; Zhang, L.; Chen, X. *In Situ* shRNA Synthesis on DNA-Polylactide Nanoparticles to Treat Multidrug Resistant Breast Cancer. *Adv. Mater.* **2018**, *30*, 1705737.
(54) Meng, F.; Zhong, Z.; Feijen, J. Stimuli-Responsive Polymersomes for Programmed Drug Delivery. *Biomacromolecules* **2009**, *10*, 197−209.

DOI: 10.1021/acsnano.9b07212
ACS Nano 2020, 14, 620−631